14th International Symposium on Turbulence and Shear Flow Phenomena (TSFP14)
Heidelberg, Germany, July 28–31, 2026

ADJOINT-BASED THERMAL SOURCE ESTIMATION IN BUOYANCY-AFFECTED TURBULENT FLOWS IN COMPLEX CHANNELS

Yukinori Kametani
Dept. Mechanical Engineering Informatics
Meiji University
1-1-1 Higashimita, Tama-ku, Kawasaki, Kanagawa 214-8571, JAPAN
kametaniy@meiji.ac.jp

ABSTRACT

An RANS-DNS hybrid adjoint-based thermal source estimation algorithm for turbulent buoyant flows in complex geometries is proposed. The location of the scalar source is estimated using local scalar concentrations measured by sensors uniformly distributed along the wall surfaces. The cost functional for the adjoint optimization is defined to minimize the error between the estimated and true scalar concentrations at the sensor locations. The complex geometry is represented by the immersed boundary method, and buoyancy is incorporated via the Boussinesq approximation.

In the proposed RANS-based algorithm, ground-truth turbulent statistics are first obtained. The eddy diffusivity used in the adjoint analysis is computed from the ground-truth turbulence statistics using the Boussinesq approximation. In this study, the ground-truth statistics are obtained from direct numerical simulation (DNS) in place of experimental measurements.

The proposed algorithm is applied to a turbulent channel flow where a scalar source is located on the bottom wall. It is found that, due to buoyancy effects, the cost functional—i.e., the estimation error—is further reduced. This is because the scalar is more likely to reach the sensors on the upper wall, thereby enabling the adjoint scalar field to be more appropriately generated there. As a result, the sensitivity becomes more accurate, improving the estimation performance.

INTRODUCTION

Scalar quantities such as toxic gases or heat are transported by convection in fluid flows. In emergency situations involving gas leaks or localized high-temperature sources such as fires, rapid and accurate identification of the source location is critical. However, scalar source estimation in turbulent flows remains a challenging task due to the complex and chaotic nature of turbulent convection.

Various methods have been proposed for scalar source estimation, including forward modeling, backward reconstruction, and stochastic approaches (see review in Liu & Zhai (2007)). With the recent advancement in AI technologies, Hosseini et al. Hosseini & Shiri (2024) proposed a physics-informed neural network framework for reconstructing flow fields. Meanwhile, adjoint-based scalar source identification has attracted attention because of its computational efficiency and accuracy. For instance, Wang et al. Wang et al. (2019) applied an unsteady adjoint analysis to scalar transport in turbulent channel flow, where the scalar was released from a steady source. They discussed the impact of sensor and source placement on the accuracy of source identification.

One limitation of unsteady adjoint analysis is the restricted time horizon due to the linearization of the governing equations, which becomes problematic for temporally growing scalar fields. To address this, Kametani et al. (2020) proposed a DNS-informed RANS-based steady adjoint framework for turbulent flow optimization, in which eddy viscosity and diffusivity were derived from DNS to improve estimation accuracy.

In thermally driven flows, scalar (heat or mass) transport is significantly influenced by buoyancy due to fluid density variations. For example, in tunnel fire scenarios, smoke tends to rise toward the ceiling and is advected depending on the strength of the buoyancy force Tan et al. (2017).

In this study, we develop a DNS-informed RANS-based adjoint optimization algorithm for estimating scalar (heat) source locations in buoyancy-driven turbulent flows. The proposed method is applied to a turbulent channel flow to investigate how buoyancy affects the accuracy of source estimation.

PROBLEM SETTING

Computational domain

A point scalar source is assumed to be located on the lower wall of a turbulent channel flow, as illustrated in Fig. 1. The computational domain dimensions in the streamwise (x), wall-normal (y), and spanwise (z) directions are set to $(L_x, L_y, L_z) = (4\pi, 2, \pi)$, with corresponding grid resolutions of $(N_x, N_y, N_z) = (256, 128, 96)$. Temperature sensors are uniformly distributed on the bottom wall. The true location of the scalar source is noted as $\mathbf{x}_s^{\text{true}}$. For the velocity field, periodic boundary conditions are applied in the x- and z-directions, while no-slip boundary conditions are imposed at the walls. For the temperature field, a Dirichlet (zero temperature) condition is applied at the inlet (upstream), and zero-gradient (Neumann) conditions are applied on all other boundaries.

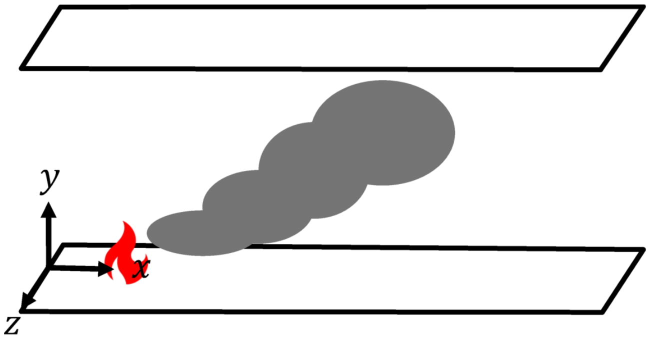

Figure 1. Schematics of flow: Heat source and buoyant flow

Ground-truth computation

In this study, experimental measurement data are replaced with data obtained from direct numerical simulation (DNS). The governing equations are the incompressible continuity equation, the Navier-Stokes equations, and the scalar transport equation, given as follows:

$$\nabla \cdot \mathbf{u}_T = 0 \tag{1}$$

$$\frac{\partial \mathbf{u}_T}{\partial t} + (\mathbf{u}_T \cdot \nabla)\mathbf{u}_T = \frac{1}{Re}\nabla^2 \mathbf{u}_T - \nabla p_T + Ri\,\theta_T\,\delta_{i2} - \eta \mathbf{u}\psi \tag{2}$$

$$\frac{\partial \theta_T}{\partial t} + (\mathbf{u}_T \cdot \nabla)\theta_T = \frac{1}{Re\,Pr}\nabla^2 \theta_T + \phi_T - \eta\,\theta_T\,\psi \tag{3}$$

The equations are nondimensionalized using the bulk mean velocity U_b^*, the channel half-width δ^*, and a reference scalar concentration θ_τ^* associated with the scalar source. Here, the superscript * denotes dimensional quantities, and ϕ_T represents the ground-truth scalar source, modeled as a Gaussian kernel. The last terms in the Eqs. (2) and (3) are volume penalization terms to achieve no-slip and isothermal condition in the solid. ψ is the phase indicator which takes 1 in the solid and 0 in the fluids.

The Reynolds number, defined by U_b^*, δ^*, and the kinematic viscosity ν^*, is set to 2800. The Prandtl number is set to unity, assuming a gas-phase fluid. The Richardson number Ri represents the magnitude of the buoyant force and several values are examined to investigate effect on accuracy of estimation.

The spatial discretization is based on a second-order energy-conservative central finite difference scheme. For time integration, a third-order Runge-Kutta method is used for the convective terms, and a second-order Crank-Nicolson method is applied to the diffusive terms. Velocity and pressure are coupled using the SMAC (Simplified Marker and Cell) method. The pressure Poisson equation is solved using a fast Fourier transform (FFT) in the streamwise and spanwise directions.

Immersed boundary for complex geometry

Complex geometries are expressed by a level-set function ψ_0 representing the signed distance from the fluid-solid interface as shown in Figure 2.

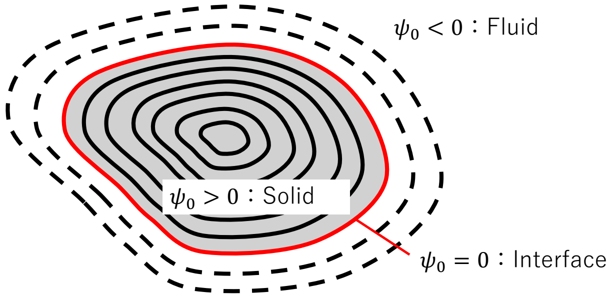

Figure 2. Fluid-solid interface with levelset function

ADJOINT-BASED SOURCE ESTIMATION

Adjoint analysis

The forward equation, serving as the constraint in the adjoint optimization, is the Reynolds-averaged energy equation:

$$\mathscr{G} = \nabla \cdot (\overline{\theta}\overline{\mathbf{u}}) - \nabla \cdot (\alpha_{\mathrm{eff}} \nabla \overline{\theta}) - \phi + \eta \overline{\theta} \psi = 0. \tag{4}$$

Here, θ denotes estimated temperature. The effective diffusivity α_{eff} consists of molecular and eddy diffusivities, viz. $\alpha_{eff} = \alpha + \alpha_\tau$. The cost functional $\mathscr{J}$ for adjoint optimization is defined to minimize the error between the estimated and true scalar concentrations at the sensor locations as,

$$\mathscr{J} = \int_\Omega \frac{1}{2}(\overline{\theta}(\mathbf{x}_m) - \overline{\theta}(\mathbf{x}_m))^2 \mathrm{d}V, \tag{5}$$

where $\mathbf{x}_m$ denotes the sensor positions.

By combining the cost functional $\mathscr{J}$ and the constraint $\mathscr{G}$ via the adjoint variable (adjoint temperature) $\theta^\dagger$, the Hamiltonian $\mathscr{H}$ is constructed as

$$\mathscr{H} = \mathscr{J} - \langle \theta^\dagger, \mathscr{G} \rangle, \tag{6}$$

where $\langle , \rangle$ denotes the inner product.

Taking the Fréchet derivative of $\mathscr{H}$ with respect to the scalar source ϕ, the infinitesimal variation of the Hamiltonian $\mathscr{H}'$ due to the one of estimated scalar source ϕ' can be expressed as

$$\frac{\mathscr{D}\mathscr{H}}{\mathscr{D}\phi}\phi' = \mathscr{H}' = \mathscr{J}' - \langle \theta^\dagger, \mathscr{G}' \rangle \tag{7}$$

$$= \langle \theta', \mathscr{G}^\dagger \rangle + \mathscr{B} + \mathscr{S}, \tag{8}$$

where

$$\mathscr{G}^\dagger = \nabla \cdot (\overline{\theta^\dagger}\overline{\mathbf{u}}) - \nabla \cdot (\alpha_{\mathrm{eff}} \nabla \overline{\theta^\dagger}) - \phi^\dagger \tag{9}$$

$$\mathscr{B} = \int_\Gamma \left(\alpha_{eff}\theta^\dagger \nabla \theta' + \alpha_{eff}\theta' \nabla \theta^\dagger \right) \cdot \mathbf{n}\mathrm{d}S \tag{10}$$

$$\phi^\dagger = \overline{\theta}(\mathbf{x}_m) - \overline{\theta}(\mathbf{x}_m). \tag{11}$$

Solving adjoint equation, $\mathscr{G}^\dagger = 0$ with appropriate boundary conditions which satisfies =0, the sensitivity $\mathscr{S}$ is obtained as

$$\mathscr{S} = \frac{\mathscr{D}\mathscr{H}}{\mathscr{D}\phi} = -\theta^\dagger. \tag{12}$$

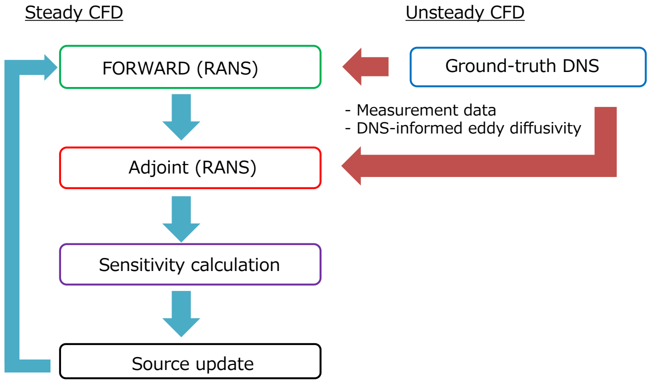

Figure 3. Flowchart of scalar source estimation

Based on the sensitivity, the estimated source is iteratively updated as

$$\phi^{m+1} = \phi^m + \beta\theta^\dagger, \tag{13}$$

where β is a constant.

DNS-informed eddy diffusivity

In this study, the eddy diffusivity α_τ is calculated from turbulent statistics obtained from the ground-truth simulation using the Boussinesq approximation,

$$-\overline{\theta''\mathbf{u}''} = \alpha_\tau \nabla\overline{\theta} \tag{14}$$

By taking the dot product with the mean temperature gradient, the eddy diffusivity is estimated so as to reproduce the local production of thermal fluctuations as

$$-\overline{\theta''\mathbf{u}''}\cdot\nabla\overline{\theta} = \alpha_\tau \nabla\overline{\theta}\cdot\nabla\overline{\theta}. \tag{15}$$

Procedure of optimization

In the algorithm, three sets of numerical simulations are conducted: a ground-truth simulation to obtain measurement data for the mean velocity, temperature, and turbulent heat flux; a forward energy simulation based on the Reynolds-averaged energy equation with the estimated scalar source; and an adjoint energy simulation to calculate the sensitivity used to update the estimated source. The forward-adjoint cycle is iterated until the cost functional converges.

The DNS-informed eddy diffusivity enables high-fidelity reproduction of turbulent heat fluxes in the RANS-based adjoint optimization framework without requiring any tuning of turbulence model parameters. The flowchart of the optimization is shown in Figure 3

RESULTS AND DISCUSSION

Estimation in the plane channel

The algorithm was applied to a simple plain channel geometry, and the estimation performance was evaluated for cases with $Ri = 0, 0.4$ and 3. The true location of the scalar source, $\mathbf{x}_s^{\mathrm{true}}$, is set to $(2, 0, 0.5\pi)$. The isosurface of temperature at $Ri = 3$ is depicted Fig. 4

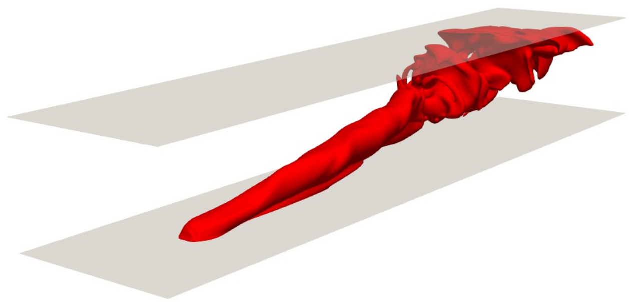

Figure 4. Isosurface of ground-truth temperature at $Ri = 3$ ($\theta_T = 1$)

Table 1. Buoyant dependency on the estimation accuracy

Ri	Distance
0	9.8×10^{-2}
0.4	4.9×10^{-2}
3.0	0.0×10^{-2}

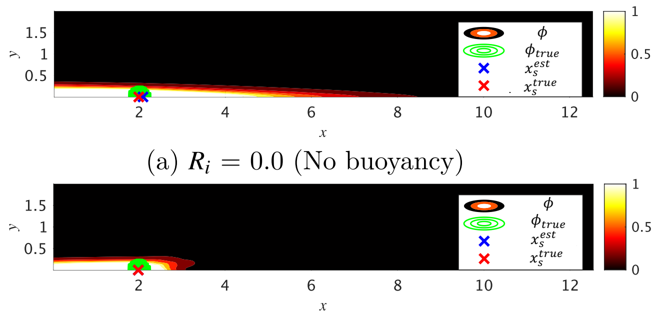

(a) $R_i = 0.0$ (No buoyancy)

(b) $R_i = 3.0$

Figure 5. Estimated source, ϕ

The cost functionals $\mathscr{J}$, defined as the estimation error, were 0.3 and 0.1 for $Ri = 0$ and 3, respectively. This indicates that the estimation performance improves in buoyant flows.

The estimated scalar source in the $x-y$ plane above the true source location $\mathbf{x}_s^{\mathrm{true}}$is shown in Figure 5. It is evident that ϕ becomes more localized in the presence of buoyancy. The accuracy of source localization is evaluated by the distance between the true location of the scalar source and location of maxima of the estimated source. The dependency of the Richardson number on the accuracy is listed in Table 1. It is apparent that, as Ri increases, the prediction of estimation becomes moreaccurate. This is because the scalar is more likely to reach the sensors on the upper wall, allowing the adjoint scalar to be released there effectively as shown in Figure 6. As a result, the sensitivity becomes more accurate, leading to improved estimation performance.

Estimation in the channel with a cylinder

As the second optimization example, the cylinder is set between two parallel walls as shown in Figure 7. The diameter of the cylinder scaled by the channel-half width is set to be 0.5. The sensors are uniformly added in the

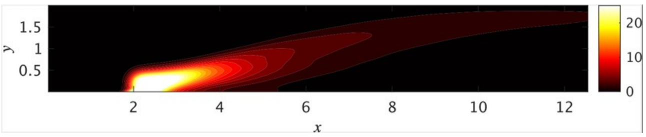

Figure 6. Ground-truth temperature at $Ri = 3$ in $x - y$ plain.

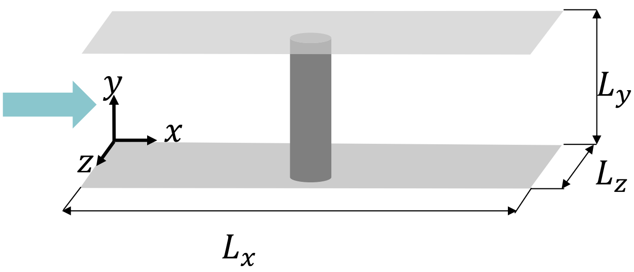

Figure 7. Flow geometry with a cylinder

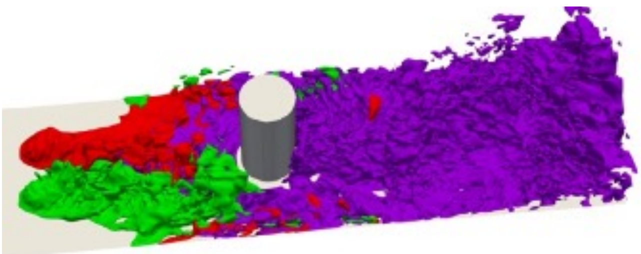

Figure 8. Example of scalar convection around the cylinder

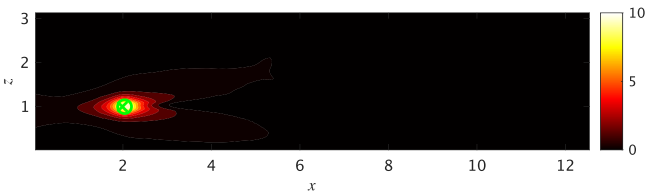

Figure 9. Localization due to the varied stream cylinder. Contour, estimated source; o, true source position; x, estimated position.

surface of the cylinder. The true location of the scalar source, $\mathbf{x}_s^{\text{true}}$, is set to $(x, y, z) = (2, 0, 1)$. The Richardson number for the buoyancy is set to 3. The example of scalar transport in this set-up is visualized in Figure 8.

The estimated source is depicted in Figure 9. Comparing with the Figure 5, remarkably, the spatial distribution of the estimated heat source is more localized. It should be noted that the mean stream is bended by the cylinder and the convection is not along the streamwise direction (x-). This fact leads the adjoint temperature gathers near true source from different directions and the sensitivity distributes in narrow region. As a result, the estimated source is localized.

CONCLUSION

DNS-informed RANS-based adjoint analysis is applied to scalar source estimation in turbulent channel flows with buoyancy effects. The cost functional is defined as the mean-square error between the estimated and measured temperatures. Sensors are assumed to be uniformly distributed on the wall surfaces.

First, the proposed algorithm is applied to a plain turbulent channel flow with a heat source located on the bottom wall under different buoyancy conditions, characterized by the Richardson number. The results show that higher Richardson numbers lead to improved localization accuracy of the scalar source estimation, because not only the sensors on the bottom wall but also those on the upper wall contribute effectively to the estimation through enhanced vertical thermal convection.

Second, a cylinder is introduced into the turbulent channel flow, and additional sensors are placed on the cylinder surface. It is found that the presence of the cylinder bends the mean streamlines around the object, thereby improving the localization accuracy of the source estimation.

REFERENCES

Hosseini, M. Y. & Shiri, Y. 2024 Flow field reconstruction from sparse sensor measurements with physics-informed neural network. Phys. Fluids 36, 073606.

Kametani, Y., Fukuda, Y., Osawa, T. & Hasegawa, Y. 2020 A new framework for design and validation of complex heat transfer surfaces based on ad- joint optimization and rapid prototyping technologies. J. Ther. Sci. Technol. 15, No. 2.

Liu, X. & Zhai, Z. 2007 Inverse sources of groundwater pollution: an optimization approach. Water Resour. Res. 17(6), 419–438.

Tan, F., Li, L. J., Dong, M. S., Wang, Q., Mei, F. Z. & Hu, L. H. 2017 Characterization of buoyant flow stratification behaviors by richardson (froude) number in a tunnel fire with complex combination of longitudinal ventilation and ceiling extraction. Appl. Therm. Eng. 110, 1021–1028.

Wang, Q., Hasegawa, Y. & Zaki, T. A. 2019 Spatial reconstruction of steady scalar sources from remote measure- ments in turbulent flow. J. Fluid Mech. 870, 111–147.